ELSEVIER

Tectonophysics 274 (1997) 145–169

TECTONOPHYSICS

An interpretation of the active deformation of southern Taiwan based on numerical simulation and GPS studies

Jyr-Ching Hu [a,*], Jacques Angelier [b], Shui-Beih Yu [a]

[a] *Institute of Earth Sciences, Academia Sinica, P.O. Box 1-55 Nankang, Taipei, Taiwan*
[b] *Dépt Géotectonique, URA 1759, Univ. P. and M. Curie, 4 pl. Jussieu, T26-E-1, 75252, Paris, Cedex 05, France*

Received 15 April 1996; accepted 24 July 1996

Abstract

The fold-and-thrust belt of Taiwan results from oblique convergence between the Eurasia and the Philippine Sea plate, and its front structures are strongly influenced by the presence of large horsts and basins in the foreland. Using a 2-D numerical modelling (finite-element and distinct-element methods), we evaluate the influences on the active deformation of southern Taiwan of: (1) the foreland structural highs; (2) the major fault zones in the belt; and (3) the presence of a subduction zone to the south. To constrain our models, we take into account for the first time the present-day velocity field of southern Taiwan estimated based on new geodetic data obtained through the Global Positioning System (GPS). Particular attention is paid to the role of geological discontinuities, through an evaluation of the presence and role of mechanical decoupling along major faults, which plays an important role in the distribution of the regional and local velocity and stress patterns. This particular analysis of the behaviour and influence of weak shear zones in Taiwan is carried out by using, for the first time, the distinct-element method. Additional 3-D distinct-element modelling allows better consideration of oblique shearing, such as for the Longitudinal Valley Fault of eastern Taiwan. We conclude that the active velocity field and tectonic stress pattern in southwestern Taiwan strongly depend on: (1) the presence and shape of the Peikang High; (2) the presence of the major active regional discontinuities (the Longitudinal Valley Fault and the major thrusts of western Taiwan); and (3) the neighbouring weakness zone of the accretionary prism of the northern Manila subduction zone, and cannot be explained by any of these factors taken solely.

Keywords: numerical models; global positioning system; deformation; Taiwan

1. Introduction

The Taiwan mountain belt is an active curved collision belt and thrust wedge which developed as the result of the late Cenozoic oblique convergence between the Philippine Sea plate and the Eurasian plate (Suppe, 1984; Barrier, 1985; Angelier, 1986; Ho, 1986; Tsai, 1986; Teng, 1990; Lu and Hsü, 1992). This collision zone connects the south-vergent Ryukyu subduction zone, where the Philippine Sea plate is subducting beneath the Eurasian plate, and the west-vergent Manila subduction zone, where the Philippine Sea plate is overriding the crust of the South China Sea (Fig. 1). The fold-and-thrust belt of Taiwan advanced northwestward, while the orogen growth was propagating southwestward along the passive continent margin of the Eurasian plate (Suppe, 1984).

* Corresponding author. E-mail: jchu@earth.sinica.edu.tw

PII S0040-1951(96)00302-2

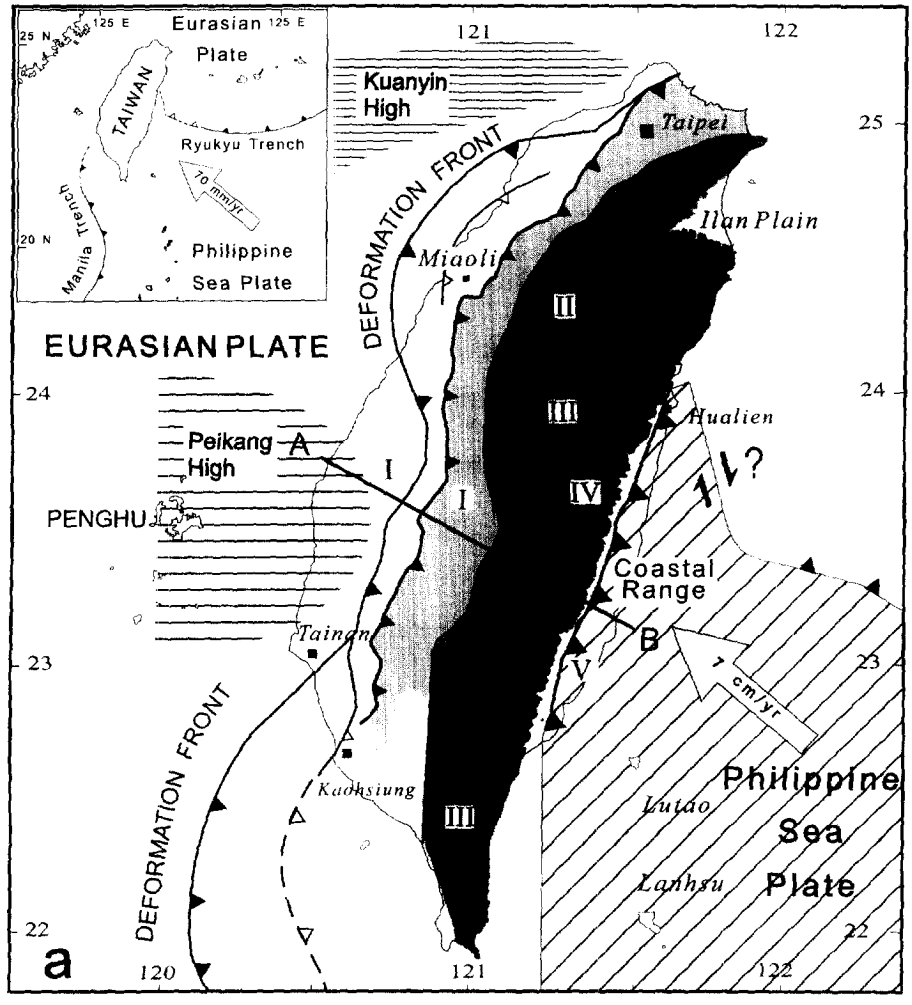
Eurasian Plate
TAIWAN
Ryukyu Trench
Manila Trench
Philippine Sea Plate
EURASIAN PLATE
Kuanyin High
Peikang High
PENGHU
DEFORMATION FRONT
DEFORMATION FRONT
Miaoli
Taipei
Ilan Plain
Hualien
Coastal Range
Tainan
Kaohsiung
Lutao
Lanhsu
Philippine Sea Plate
I
II
III
IV
V
A
B
a
b
Unit I
Coastal Plain
Western Foothills
Central Range = Unit II + III + IV
Slate Terrain
Tananao Complex
Coastal Range
Unit V
LVF
0 10 20 30 km
Pliocene-Quaternary Sequence
Miocene Sequence
Mesozoic Basement
Miocene Slate
Paleogene Slate
Schist Complex
Neogene Melange
Neogene Volcanics
LVF Longitudinal Valley Fault

Extensive palaeostress analyses have been made throughout the island of Taiwan during the last 10 years, so that the evolution of tectonic palaeostresses is better known in terms of regional distribution, nature and major trends (Barrier, 1985, 1986; Barrier and Angelier, 1986; Angelier et al., 1986, 1990; Lee, 1986; Chu, 1990; Lacombe et al., 1993; Rocher et al., 1996). Such local palaeostress determinations allowed not only the description of local mechanisms, but also the understanding of regional tectonics at the scale of the plates. The regional knowledge of the late Cenozoic palaeostress field thus provides strong constraints in the geodynamic interpretation of the Taiwan collision belt. However, the consistency between the deformation at the regional scale and the reconstructed palaeostress patterns remained poorly analysed in general, despite its importance in tectonics and geodynamic studies.

In order to address the problem of the consistency between palaeostress and deformation, it is necessary to carry out numerical modelling of strain–stress relationships. Such modelling allows quantitative evaluation of the compatibility between kinematic boundary conditions, geological structure and palaeostress patterns. This modelling may involve various techniques, depending on the type of deformation.

Ten years ago, based on the available structural and tectonic knowledge of the Late Cenozoic collision in Taiwan, and taking into account the independent information on the kinematics of the Philippine Sea plate relative to Eurasia (Seno, 1977; Minster and Jordan, 1979; Ranken et al., 1984; Huchon, 1986; DeMets et al., 1990), a viscous 2-D finite-element model was proposed by Huchon et al. (1986). It included consideration of different rheological domains and a discussion of the role of variable boundary conditions. This first numerical model of the Taiwan collision aimed at simulating a rigid body (the Luzon Arc) indenting into a rigid–plastic material (the Chinese continental margin).

Recently, Hu et al. (1996) presented a new 2-D plane stress elastic and elasto–plastic finite-element model, for both the Taiwan orogen and the neighbouring arc-and-trench systems. This new model was built principally in order to explain and quantify the relationships between the stress distributions and the convergent kinematics that prevailed in the whole subduction and collision zones in and around Taiwan during the Plio–Pleistocene. Despite large differences in the sizes of the domains considered, the structure and rheological characteristics of the models, and the level of the geological and geophysical knowledge used to constrain modelling experiments, both Huchon et al. (1986) and Hu et al. (1996) simulated the stress regimes and trajectories in the Taiwan region by using finite-element methods. Although zones with special rheological properties were introduced in the second model in order to account for the mechanical decoupling at trenches, these studies were made with the usual concepts of continuous media. By definition, the particular mechanical properties of the deforming lithosphere related to the presence of major zones of weakness where shear concentrates were not taken into rigorous account.

For instance, in both these models, the slip component along the Longitudinal Valley Fault of eastern Taiwan was ignored, although this major fault zone plays a significant role in the deformation of Taiwan (Tsai, 1986; Ho, 1986; Barrier and Angelier, 1986; Yu and Liu, 1989; Yu et al., 1997). The Longitudinal Valley Fault is the surface expression of a major shear zone striking N20°E, dipping approximately 55° to the ESE, which can be followed along strike over a distance of about 160 km, and along dip at depths of more than 45 km. The amount of oblique slip on this fault zone is larger than 3 cm/yr, combining thrusting and left-lateral slip. Other major shear zones are present throughout the Taiwan mountain belt, also playing a significant role in the distribution of stress and strain. As a result, the general finite-element models, which are of large interest for describing the overall behaviour of the collision zone, fail to represent the actual stress–strain situation in the vicinity of the major mechanical discontinuities where slip occurs.

Tectonic processes which affect a geologically homogeneous area produce regular trends in stress

Fig. 1. (a) Tectonic framework and main structural units in Taiwan (geodynamic setting in the upper-left corner). Major thrust faults with triangles on the upthrust side; *L.V.* = Longitudinal Valley; *I* = Western Foothills and Coastal Plain; *II* = Hsüeshan Range; *III* = Backbone Range; *IV* = Mesozoic/Palaeozoic Basement; *V* = Coastal Range. (b) Schematic cross-section of Taiwan, after Teng (1990). *A–B* = location in (a).

and strain at the regional scale, so that the use of a mathematical model based on the concepts of mechanical continuity seems appropriate. However, this assumption of continuity becomes invalid where 'weak' major fault zones (that is, fault zones with little mechanical coupling) are present. When a rock mass containing a structural discontinuity is deformed in such a way that relative motion occurs across the discontinuity, the displacement, strain and stress fields may be deeply modified for both the magnitudes and the orientations. In turn, the knowledge of these 'perturbed' fields can be used in order to analyse the properties of the discontinuous active structure and regional deformation. The investigation of such perturbations in stress and deformation fields in presence of major mechanical discontinuities is thus an important aspect in the analysis of the geodynamic behaviour where major active faults are present. The regional finite-element modelling discussed before aims at minimizing and averaging these aspects throughout large deformed areas, and thus is not an appropriate tool for this particular purpose. In this paper, we especially address this problem, which requires the use of particular modelling techniques.

Two major concerns in modelling applied to analyses of geodynamic problems deal with (1) the level of detail which can be obtained in realistic conditions with the techniques adopted and the data available, and (2) the need for real consideration of geological discontinuities, which are known to play a major role in tectonics although their behaviour and influence are not satisfactorily accounted for by the classical mechanics of continuous media. It is now possible to go farther in the modelling of the collision zones, first because more sophisticated techniques are available such as for distinct-element modelling, and second because a large mass of new data is available, including a more comprehensive description of palaeostress and a new reconstruction of the present-day deformation field based on GPS studies. We consequently chose Taiwan as a case example for comparative modelling (Hu, 1995) because it provides a good opportunity for understanding the behaviour of a collision zone which undergoes active shortening and strong mechanical coupling but also includes major fault zones where mechanical decoupling is likely to occur.

A characteristic feature of the Taiwan mountain belt (Fig. 1a) is the S-shape of the general structural trends consistent with the geometry of the collision (Lu and Malavieille, 1994; Lu et al., 1995). Although a many-kilometers-thick late Cenozoic sediment mass generally fills a foreland basin in western Taiwan (Fig. 1b), two major basement highs are present: the Peikang High to the south and the Kuanyin High to the north (Fig. 1a). Drilling and seismic-reflection data outlined the semi-circular shape of the Peikang High, which is characterized by its tectonic stability, in contrast to the adjacent mobile belt. The presence of such a crustal mass is likely to play an important role in the development of the front fold-and-thrust belt. The southern Taiwan area includes both the southern propagating tip of the collision belt and the northern onland extension of the accretionary wedge between the Manila Trench and the North Luzon Trough and Luzon volcanic arc (Fig. 1a). Recent geological analyses offshore southern Taiwan have shown active southward propagation of the arc–continent collision (Lundberg et al., 1991; Huang et al., 1992; Liu et al., 1993; Huang et al., 1995). The front of the major submarine fold-and-thrust zone located along the western flank of the accretionary wedge is also an important feature to consider at the southwestern tip of the collision belt.

New satellite-based geodetic surveys allowed extension of the original trilateration networks in order to cover the whole collision zone of Taiwan. Accurate geodetic data on present-day deformation thus provide a good opportunity to study the relationships between the crustal deformation and the plate kinematics. The aim of this study is to check and refine the general interpretation of the relationships between active deformation and geological structure in southern Taiwan, based on two independent numerical modelling techniques (finite- and distinct-element codes) using for the first time (Hu et al., 1995) the constraints of the deformation field revealed by GPS measurements (Yu and Chen, 1994).

2. The present-day deformation of southern Taiwan

The modelling work presented herein aims at providing a better account of the active tectonic be-

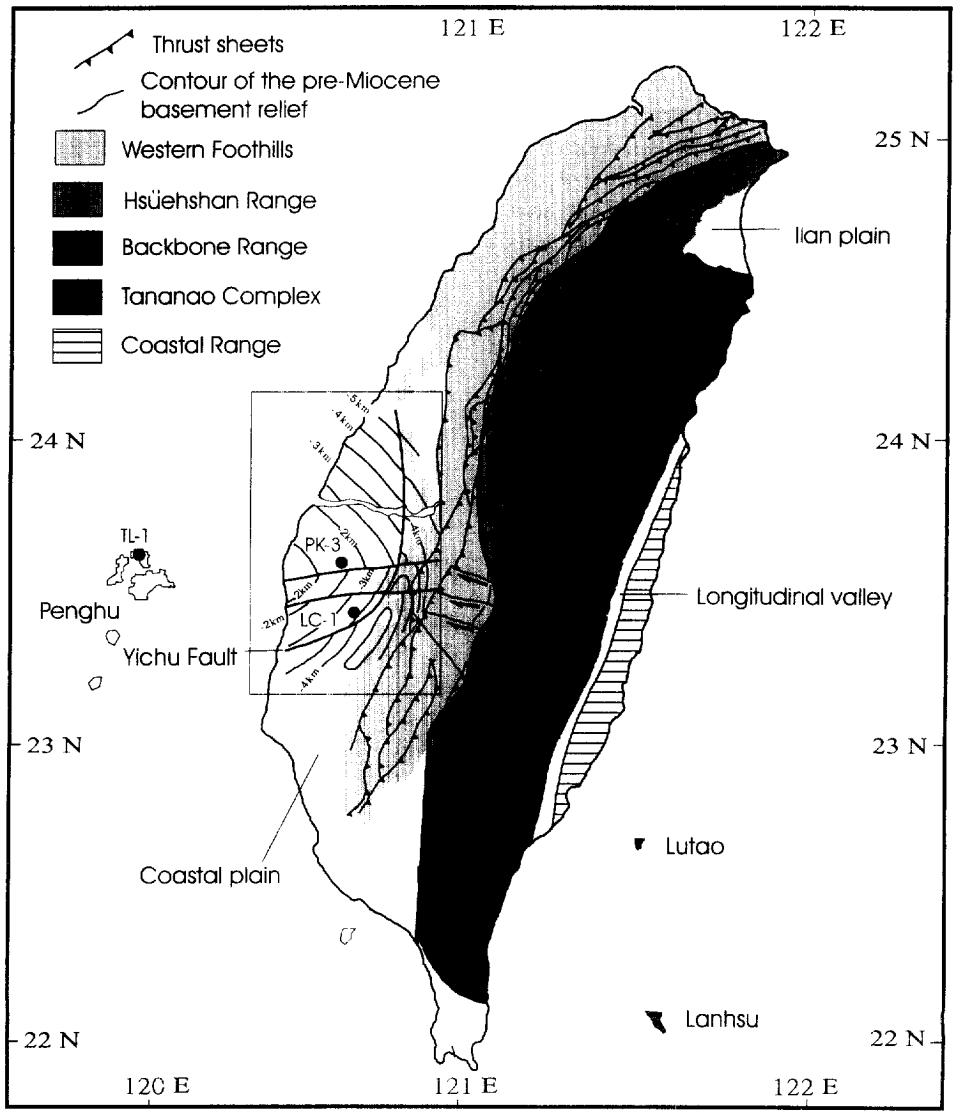

Fig. 2. Main structural units in the Peikang area (modified after Hsu and Sibuet, 1995). PK-3, LC-1, TL-1 indicate wells of CPC. Depths of pre-Miocene basement shown beneath the Coastal Plain in the Peikang High area (framed).

haviour of the major units of the Taiwan collision belt, including consideration of the role of major weakness zones where slip occurs. In this section, we focus on the main data used as major constraints in this new modelling: the geological structure (with emphasis on the sources of inhomogeneity), the regional pattern of active displacements (as revealed by recent geodetic analyses) and the stress distribution (including perturbations in trajectories). The general information on the geology of Taiwan (Figs. 1 and 2) can be found easily in three volumes of this journal (Vol. 125 in 1986, Vol. 183 in 1990, and this issue).

2.1. The geological structure

The Taiwan mountain belt (Fig. 1) developed since about 5 Ma ago as a result of oblique collision

of the Luzon island arc with the Chinese continental margin. The two main geological provinces of Taiwan are separated by the active Longitudinal Valley Fault (Ho, 1986; Tsai, 1986), hereafter referred to as LVF. To the east, the Coastal Range comprises mainly volcanic and siliciclastic sequences of the accreted Luzon arc–trench system, whereas the area to the west consists of metamorphic and sedimentary sequences of the deformed Chinese continental margin.

The Central Range of Taiwan is characterized by the presence of Tertiary metamorphism, in contrast with the adjacent non-metamorphic fold-and-thrust belt of the Western Foothills (Ho, 1986). The pre-Tertiary basement, which has been affected by Neogene greenschist facies as well as by higher grades of polyphase Mesozoic–Cenozoic metamorphism, crops out in the eastern flank of the Central Range. The axial ridges and the western flank constitute the Slate Belt. In the Western Foothills, the Miocene, Pliocene and Early Pleistocene shallow-marine to shelf clastics sediments are affected by WNW-vergent folds and low-angle thrust faults. The Coastal Plain of western Taiwan and offshore areas further to the west are underlain by mostly flat-lying Cenozoic sedimentary sequences which have not yet been deformed by the collision (Fig. 1b). The Coastal Plain is composed of Quaternary alluvial deposits derived from the Central Range and the Western Foothills.

A major basement high, the Peikang High, is present in the foreland at the front of the belt (Fig. 1a). It deserves particular consideration because of its tectonic role as a relatively rigid indenter (Lu, 1994) relative to the fold-and-thrust belt (Fig. 2). The Peikang High belongs to the continental lithosphere of Eurasia which underwent normal faulting prior to collision. Its existence was revealed by subsurface studies. The geophysical survey and drilling by the Chinese Petroleum Corporation (hereafter CPC) resulted in the discovery of the Peikang Massif beneath the Neogene sediments: two wells (PK-2 and PK-3) penetrated the basement, with Cretaceous metamorphic rocks, at depths of 1463 m and 1962 m, respectively (Matsumoto, 1965). A well (TL-1) drilled in the Penghu Islands revealed a similar occurrence of mid-Miocene sediments unconformably overlying a Mesozoic basement at a depth of 500 m (Chou, 1969), showing that the main Penghu Islands belong to the offshore extension of the Peikang Massif. The shape of the basement high, from Peikang to the Penghu Islands, was illustrated by a Bouguer gravity anomaly map (Hsieh and Hu, 1972).

The structure of the Peikang High is controlled by large normal faults (Yang et al., 1991). The seismic surveys showed major blocks separated by a N065°E-trending normal fault zone interpreted as a hinge fault (Stach, 1957), a rapid transition from a shelf (to the north) to a deep basin (to the south). As shown in the seismic structure-contour map of the Orbitoid limestone (Elishewitz, 1963), the strata dip gently to the northeast with little structural disturbance north of this Peikang Fault zone, whereas south of it the strata dip to the SSE and are cut by several antithetic faults before reaching the Yichu hinge-line fault zone, regarded as the southern marginal fault of the Peikang shelf (Fig. 2). South of the Yichu Fault zone, the Mesozoic basement is greatly down-faulted, as evidenced by one well (LC-1) of the CPC which, at a depth of 2600 m, was still in Pliocene sediments (Sun, 1965; Meng, 1967; Chiu, 1973; Huang, 1978).

Of particular interest is the eastern extension of the Peikang High, in the belt front zone (Fig. 2). East of the Peikang Massif, the Neogene sediments thicken from about 1500 m near Peikang to more than 6000 m only 30 km further east. The Peikang Massif, therefore, extends only at a short distance eastward beneath the front belt of west-central Taiwan.

The accretionary wedge southwest off Taiwan is also of particular interest, because it represents a particular zone of weakness related to the northernmost extension of the Manila subduction zone. In southwestern Taiwan, the deformed rock sequences of the collisional orogen can be traced offshore (Fig. 1a), in the transition zone between the Manila Trench and the front of the Taiwan arc–continental collision belt. The frontal portion of the submarine fold-and-thrust belt is located along the western flank of the accretionary wedge. Oceanographic surveys providing side-scan sonar images and seismic reflection profiles revealed a strong structural fabric with NW–SE trends offshore southwest of Taiwan, with a transition to N–S trends further south (Lundberg et al., 1991; Liu et al., 1993).

2.2. The geodetic data

For studying the present-day crustal deformation in the Taiwan area, the 'Taiwan GPS Network' was established in 1989 by the Institute of Earth Sciences, Academia Sinica (Fig. 3a). This 270-km wide network was composed of 140 stations covering Taiwan and five surrounding islands (Yu and Chen, 1994; Yu et al., 1997). The southern subnetwork considered in this paper included 78 stations, from two islands of the Penghu Archipelago, Paisha and Chimei (S01R and S002 in Fig. 3b), to the islands of Lutao and Lanhsu southeast off Taiwan (S063 and S102 in Fig. 3b). These couples of islands at the western and eastern tips of the network are of interest, because Paisha and Chimei belong to the geologically stable shelf of the continent whereas Lutao and Lanhsu belong to the Luzon Arc, hence to the Philippine Sea plate.

Changes in baseline length derived from GPS measurements provided accurate estimates of the station velocities in the active collision zone. In addition to temporary stations, four continuously recording permanent GPS stations at Paisha, Penghu (S01R), Taipei (T986 or TAIW), Pingtung (S23R) and Lanhsu (S102), as well as five semi-permanent GPS stations at Changping (S058), Minhsiun (S103), Nankang (S101), Fushan (S104) and Mingyeh (S105), were employed (Fig. 3a). The southern half of the network was surveyed five times from 1990 to 1994, with dual-frequency geodetic GPS receivers (Trimble 4000 SST Geodetic IIP and 4000 SSE Geodetic Surveyor). A station is usually occupied by more than two sessions, each session being composed of a 6–14 h of GPS observations with all available satellites rising higher than a 15° elevation angle being tracked. All available temporary measurements and continuous recordings of GPS data were processed with the Bernese GPS software (v.3.4) developed at the Astronomical Institute of the University of Berne (Rothacher et al., 1993). For each session, the baseline solutions were obtained for all possible couples of stations. Daily solutions were computed for permanent GPS stations. The ionosphere–free linear combination of observations at the L1 and L2 frequencies was employed for estimating the station coordinates and baseline solutions.

The dispersion of series of GPS measurements taken over several years provides an indicator of precision. This may be done by assuming that steady motion occurred between stations during the five-year period, and looking at the scatter of data points around the best fit straight line on a plot of the baseline component versus time (Davis et al., 1989). The long-term repeatability shows the effects of slowly varying systematic errors due to propagation delay, multipath, fiducial network inconsistencies, and so on. A datum point for each baseline is the average of all observations within 30 days. Accordingly, the repeatability of a baseline component (east, north, and vertical) or baseline length is given by the root-mean-square scatter about the linear trend. For baseline lengths up to 120 km, the standard deviations were in the ranges 5–9 mm for the length, 5–10 mm for the north component, 7–13 mm for the east component and 22–43 mm for the vertical component.

Several earthquakes with magnitudes larger than 5.0 occurred in the Taiwan region during the observation period 1990–1994. However, it seems that they had no significant influence on the length changes of the baselines. This observation supports the assumption of a steady motion occurring between the GPS stations during the five years of this GPS study.

The average rates of relative displacement for the north and east components of the baseline between the two permanent GPS stations at Paisha, Penghu (S01R) and Taipei (T986) are only 0.5 ± 0.1 mm/yr and 1.0 ± 0.4 mm/yr, respectively. In other words, the relative horizontal motion between these two stations is not significant. Considering this and the relative geological stability of the Penghu area, the coordinates of Paisha station (S01R) and the azimuth from Paisha to Taipei (N52.1°E) were fixed in the least-square adjustment to estimate the station velocities. This procedure was compulsory for resolving the translational and rotational ambiguities of the whole network in the estimation which follows. Derived velocity vectors and their confidence ellipses are shown in Fig. 3.

The displacement vectors relative to the Chinese margin increase toward the south (Fig. 3b), consistent with the geological evidence that the collision tectonics in Taiwan is migrating from north to south as a result of the oblique convergence. The velocity vectors of the stations in the two eastern volcanic islands (Lanhsu and Lutao) and most of the south-

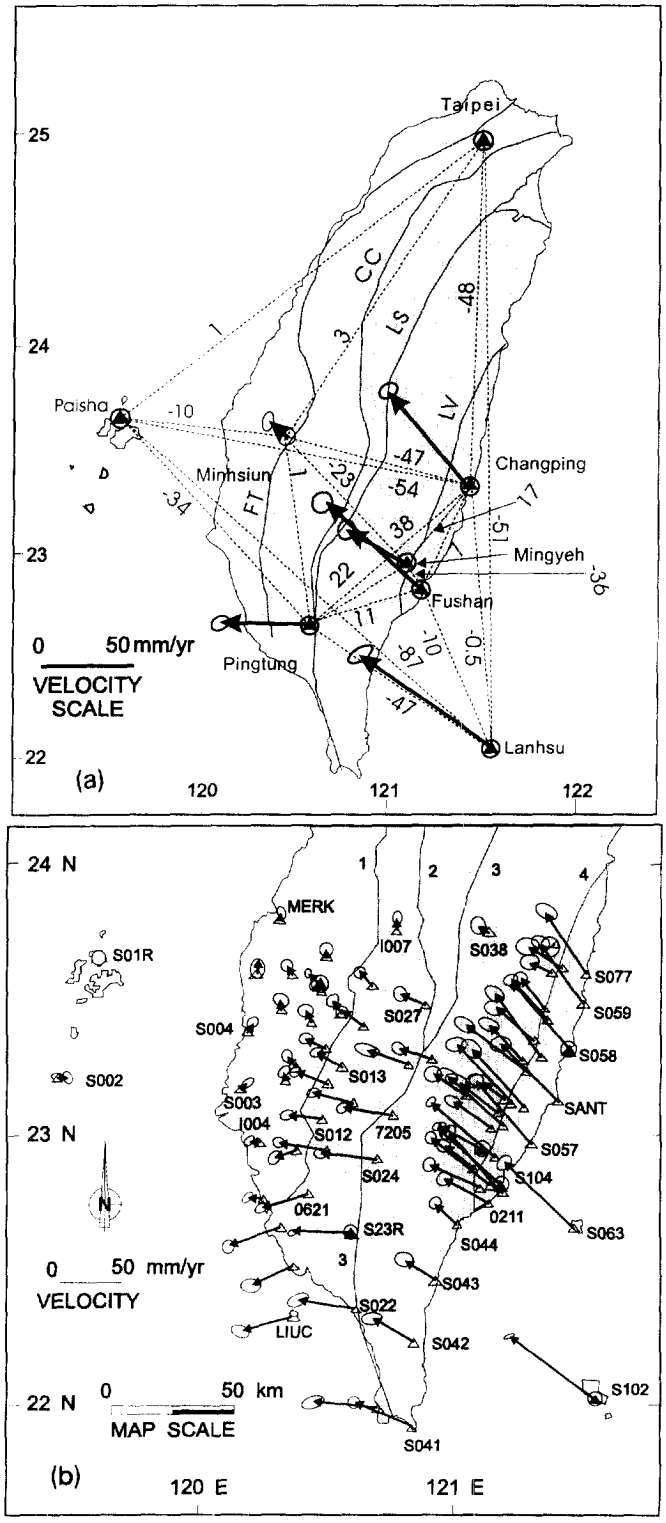
Taipei
Paisha
Minhsiun
Changping
Mingyeh
Fushan
Pingtung
Lanhsu
CC
LS
LT
FT
-10
-47
-54
-34
-51
-36
-87
-0.5
0 50 mm/yr
VELOCITY SCALE
25
24
23
22
120
121
122
(a)
24 N
23 N
22 N
MERK
I007
S01R
S002
S004
S027
S013
S003
I004
S012
7205
S024
0621
S23R
3
S022
LIUC
S042
S041
S038
S077
S059
S058
SANT
S057
S104
0211
S063
S044
S043
S102
0 50 mm/yr
VELOCITY
0 50 km
MAP SCALE
120 E
121 E
(b)

ern Coastal Range have N307-327°E trends and the largest amplitudes (60.0–86.3 mm/yr). The GPS-observed velocity of Lanhsu relative to Paisha is 86.3 ± 2.4 mm/yr, with an azimuth 307° ± 1° (Yu and Chen, 1994). Note that this velocity is larger than that (ca. 73.7 mm/yr) of the direction of plate convergence estimated by Seno (1977) and Seno et al. (1993). In the western region of the network, most station velocities in the Coastal Plain and western-central Taiwan are negligible (insignificant or only marginally significant).

The westward decrease in velocities across the active orogen of southern Taiwan is far from being spatially regular or even continuous, indicating that large amounts of shortening occur at relatively narrow shear zones. A major discontinuity of about 32 mm/yr in the velocity field is observed across the Longitudinal Valley (Fig. 3b). Another velocity discontinuity of 10–28 mm/yr is detected across the Chukou Fault, where remarkable strain accumulation rates are also observed (Yu and Chen, 1994). As far as the network density permits, one reconstructs a rather gradual counter-clockwise change in velocity trends across the Taiwan belt west of the LVF, from north-northwest in the eastern Central Range to west in the Western Foothills. To the southwest, in the Kaohsiung–Pingtung coastal area, the velocity vectors are even directed toward the southwest, with rates of 40–47 mm/yr.

2.3. The Quaternary stress distributions

Because we first consider the present-day kinematics of the Philippine Sea plate, the fit of our models must also take into account all stress data which reflect the most recent step in the geodynamic evolution of the Taiwan collision zone (Fig. 4). The present-day distribution of tectonic stress in southern Taiwan was obtained from two principal sources of data: the borehole breakouts analysed by Suppe et al. (1985), and the earthquakes focal mechanisms analysed by Yeh et al. (1991).

The map of maximum compressional stress trends obtained from borehole breakout data (Fig. 4a) describes the stress state in the uppermost crust of Taiwan (Suppe et al., 1985), in terms of trends of maximum compressional horizontal stress, σ_{hmax}, revealed by hydraulic fracturing experiments in Taiwan boreholes (Fig. 4a). Note that in the collision zone σ_{hmax} generally corresponds to the maximum compressional stress axis, σ_1, and trends WNW–ESE on average, while an other principal stress axis, σ_2 or σ_3, is nearly vertical (strike-slip faulting or reverse faulting mode, respectively).

Yeh et al. (1991), using the stress tensor analysis developed by Angelier (1979, 1984) and grouping data on earthquakes focal mechanisms from 1972 to 1986 in several regions, reconstructed the different stress regimes in the crust of the Taiwan area and obtained the orientations of the three principal stress axes, σ_1, σ_2 and σ_3. In Fig. 4b, the trends of σ_1 axes are shown where the corresponding seismotectonic regime is compressional (involving reverse or strike-slip faulting modes); they also indicate WNW–ESE compression on average.

The distribution of late Cenozoic palaeostresses in Taiwan also deserves consideration. It was studied in detail based on fault slip data analyses (Angelier et al., 1986, 1990; Barrier and Angelier, 1986; Lee, 1986; Chu, 1990). As discussed in these earlier papers, the regional distribution of compressional stress trajectories in Taiwan reflects the oblique indentation of the Luzon Arc into the Eurasian continental margin. Fan-shaped patterns of palaeostress trajectories were recognized (Angelier et al., 1986; Chu, 1990). These studies showed that for the compressional events of the Plio–Pleistocene collision, most trends of Quaternary compression are approximately WNW–ESE in southern Taiwan (Fig. 4c). In detail, however, significant changes have occurred with time.

In summary, all determinations of recent and present-day stress concur to indicate that the regional stress in the Taiwan region is dominated by WNW–

Fig. 3. (a) Continuous monitoring GPS network in Taiwan (after Lu, 1994, with data from Yu and Chen, 1994). Thick straight lines (with 95% confidence ellipse) are the estimated station velocities relative to Paisha. Shortening indicated between stations (value in mm/yr along dotted lines). Solid triangles inside circles are continuous monitoring fixed stations. *FT* = Foothills Thrust; *CC* = Chiuchih Fault; *LS* = Lishan Fault; *LV* = Longitudinal Valley Fault. (b) Velocity fields for all stations in southern Taiwan (after Yu and Chen, 1994): *1* = Chukou Fault; *2* = Chenyulanchi Fault; *3* = Lishan–Chaochou Fault; *4* = Longitudinal Valley Fault.

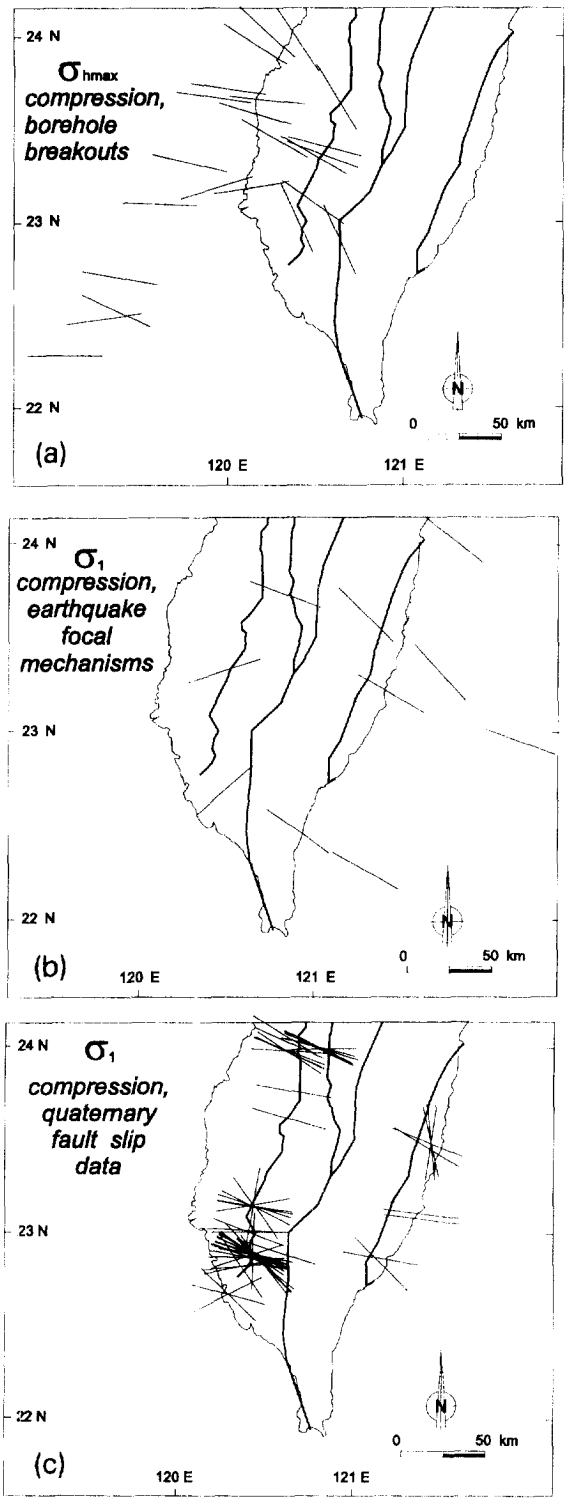

ESE compression (Fig. 4). This pattern is generally consistent with the geometry of the collision between Eurasia and the Philippine Sea plate (Fig. 1), although the reconstructions of Quaternary stress in southern Taiwan revealed systematic counter-clockwise deviation (Angelier et al., 1986) and high levels of dispersion in the direction of compression (Lacombe et al., 1993).

3. Modelling methods and mechanical discontinuities

In this section, we consider the methodological aspects of modelling through a comparison between finite-element analysis (previous studies) and distinct-element analysis (this paper). Then, we successively consider different sources of structural inhomogeneity, within the frame of numerical modelling applied to regional shortening: (1) the presence of a foreland promontory; (2) the obliquity of convergence across a non-linear boundary; (3) the existence of a neighbouring major domain of weakness related to subduction; and (4) the presence of major shear zones within the contractional belt. Through progressive addition of these effects, resulting in increasing complexity, we demonstrate that they are all necessary in order to obtain a model which satisfactorily accounts for the distribution of observed displacements reconstructed in the Taiwan mountain belt area based on GPS analyses (Fig. 3) and determinations of regional strain–stress fields (Fig. 4). Whereas finite-element modelling suffices to investigate the promontory case, distinct-element modelling is required for examining the influence of weak shear zones. We finally attempt at evaluating the consequences of the use of 2-D models where 3-D structure is involved, considering the case of a major shear zone, the LVF, which is oblique to the

Fig. 4. Present-day stress distribution in Taiwan. (a) Maximum horizontal stress orientation (σ_{hmax}) from borehole breakouts (after Suppe et al., 1985). (b) Trends of maximum compressional stress (σ_1) for twelve groups of earthquake focal mechanism data (after Yeh et al., 1991). (c) Palaeostresses related to Quaternary collision (reconstructed from fault slip data in Quaternary formation solely). Bars are trends of maximum compressional stress orientations (σ_1). After Barrier and Angelier (1986); Angelier et al. (1986, 1990); Lee (1986); Chu (1990).

Earth's surface and undergoes oblique slip (reverse and left-lateral).

3.1. Modelling method: finite element vs. distinct element

We have carried out numerical modelling for the detailed investigation of the stress and velocity fields in the collision belt and foreland around the basement high. A two-dimensional finite-element technique was used first, as for earlier studies. The geometry, material properties, and boundary conditions were chosen according to the regional geology (Figs. 1 and 2). We adapted the finite-element software 'MODULEF' developed by the French 'Institut National de Recherche en Informatique et en Automatique' (George et al., 1986). We used the very small strain approximation for the elastic model, assuming that continuous infinitesimal deformation occurs throughout the region studied, in agreement with the results of geodetic analyses. We adopted plane stress conditions, corresponding in a two-dimensional model to an 'infinitely thin' plate, where thinning or thickening is however possible.

The models used for the first-order approximation imply drastic simplification of geological patterns; they do not allow consideration of various significant stress effects due to topography, buoyancy, basal drag, coupling at depth and time- and temperature-dependent ductile mechanisms. For instance, the possible presence of a mechanically weak layer at midcrust depths in a continental lithosphere, inducing mechanical decoupling of crustal layers, is ignored. In addition, in the convergence zone, slip occurs oblique to the plate margin, between zones of strike-slip faulting and underthrusting which strike nearly parallel. Mechanical decoupling takes place along major shear zones, as perturbations in stress and velocity fields suggest. Ignoring such decoupling in finite-element modelling results in smoothing effects, which cannot account for the discontinuities observed in actual patterns.

Because we aim at understanding the mechanical behaviour of the major zones of weakness and estimating their influence on strain–stress distributions, we built new 2-D plane-strain models using the distinct-element method. As major targets, we considered the shear zones of the Longitudinal Valley and the western thrusts (Figs. 1 and 2). We adopted the distinct-element technique described by Cundall (1971, 1988) and the corresponding 'UDEC' software, because of its suitability in rock mechanical modelling of discontinuous media. The numerical analysis principles were described by Hart et al. (1988). Elastic blocks interact across their boundaries and the behaviour of planar discontinuities follows the Mohr–Coulomb law. The distinct-element modelling is based on a time marching integration scheme using central finite difference. It is an explicit method in which the equations of dynamics (e.g., Newton's second law for rigid block motion) are integrated over time.

With the distinct-element modelling, a rock mass consist of a system of discrete blocks in mechanical interaction at their boundaries. Blocks behave as deformable elastic bodies, and interactions are computed assuming finite stiffness at contact points along interfaces. The contact forces applied to rigid blocks or discrete particles (in the case of deformable blocks, a finite difference grid with mass points at vertices of tetrahedra) are given by the elastic response at contact points (stiffness both in normal and tangential directions are defined as properties of the contacts) which are evaluated after each integration cycle over the time step. Opening or shear displacement (sliding) along block interfaces occurs when the normal and the shear forces (or stress) meet conditions for tensile or shear failure, respectively. The shear strength is defined by a Mohr–Coulomb failure criterion, which requires definition of the angle of sliding friction and a cohesion as joint properties.

3.2. Major sources of regional deviations: role of promontory

Before considering the mechanical effects of mechanical discontinuities, we addressed the simpler problem of variations in rheology. A preliminary finite-element experiment (Fig. 5) illustrates the basic principle of our analysis and involves a simple symmetric 2-D model first. A highly deformable zone (the front belt) is located between two rigid blocks. One of the rigid blocks has a promontory (Fig. 5). Because rheological variations are not well constrained by geological information, we built models with a variety of values in order to explore the

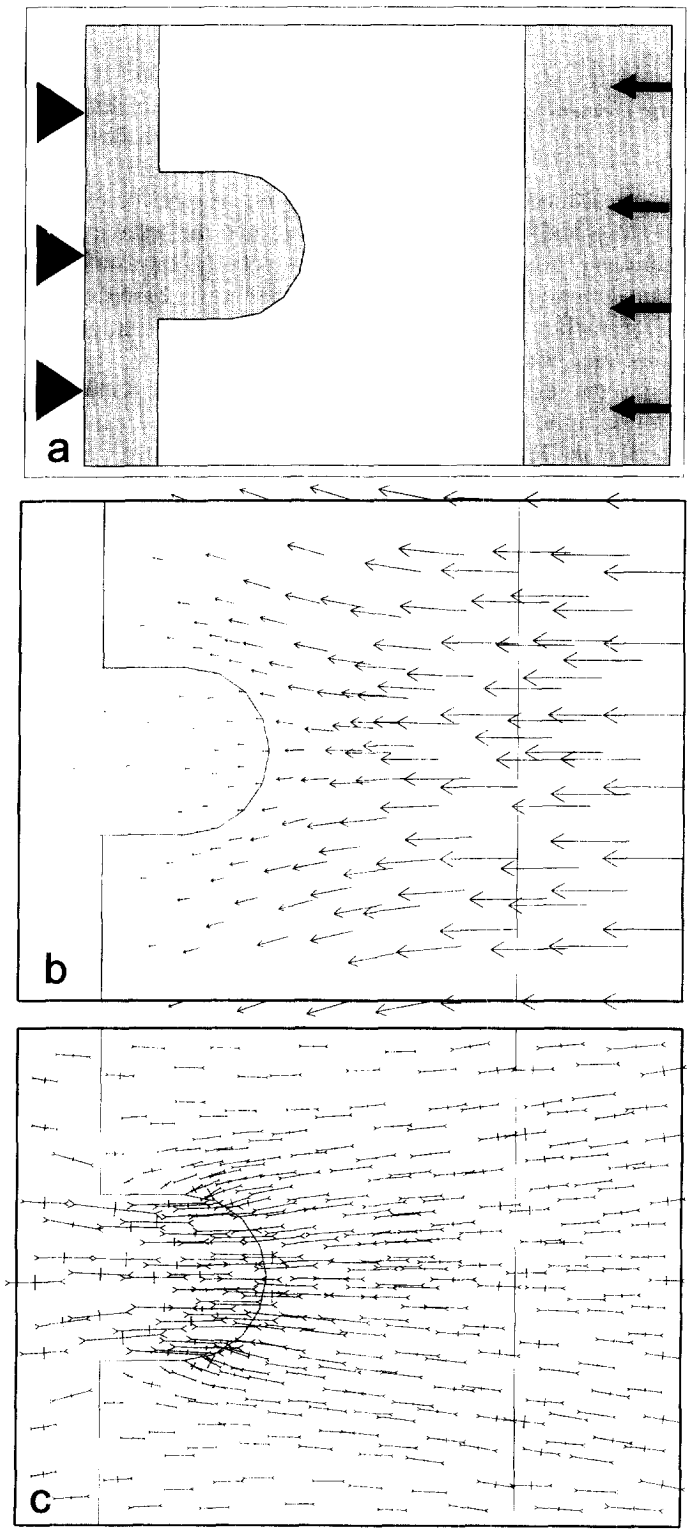
a
b
c

effects of changes in these parameters and the sensitivity of our results to their choice. The values finally retained should be regarded somewhat arbitrary. We found, however, that within acceptable ranges the patterns of stress trajectories have very little sensitivity to the absolute rheological values, and that they are moderately influenced by the ratios of these parameters.

The configuration described in Fig. 5 was designed according to the expected contrasts in rheological properties in the area under investigation (a foreland fold-and-thrust belt undergoing shortening between a 'stable' foreland and the metamorphic core of the orogen), but the geometry is quite simpler (compare Figs. 1 and 5a).

We applied an initial displacement of 0.00125% of model width on the east side and allowed no vertical displacement along the top or bottom; the western side was fixed (Fig. 5a). Such a model is able to produce a pronounced fan-shaped distribution of the velocity vectors (Fig. 5b), thereby implying that the deviation of the velocity field south of the Peikang High (Fig. 3b) may be related, at least in part, to the presence of the basement promontory. Fig. 5c shows the orientations of the maximum stress axes in this simple model: in the less resistant medium around the promontory, they slightly converge toward the promontory.

3.3. Obliquity of convergence and shape of boundary

Several models were built in order to evaluate the possible role of convergence and to adopt a realistic geometry (based on Fig. 1). One example is shown in Fig. 6. The material properties assigned to different subdomains are listed in Table 1. For boundary conditions, we have used velocities (or displacements) instead of forces (or stresses), because the latter are difficult to estimate whereas the relative motion between the Philippine Sea plate and the Chinese margin is well known (Fig. 3). The velocity imposed is 86.3 mm/yr based on the GPS results (Yu and Chen, 1994), that is, 10–15% faster than the values estimated by Seno (1977) and Seno et al. (1993). The azimuth of the displacement is 310° (i.e., N50°W), based on the latest model of Seno et al. (1993) and consistent with GPS data as discussed earlier in this paper. The dimension of the model is about 370 km × 275 km, a size sufficient to prevent edge effects in the central area of interest (southern Taiwan).

We obtained a rough fit between observed and computed velocities in the eastern half of the models (Fig. 6b). However, the deviation of the velocity vectors across the LVF was not reproduced satisfactorily in the absence of mechanical discontinuities in the model. Moreover, to the west, this model failed to satisfactorily account for the E–W and ENE–WSW trends of velocity vectors observed in southwestern Taiwan (Fig. 3b), although counter-clockwise deviation of velocity vectors is present south of the Peikang High. The actual deviation is as large as about 65° in four stations near Kaohsiung; for these stations, the computed deviation reaches 25° only, so that the misfit could not be regarded acceptable (Fig. 6b).

These discrepancies imply first that in the model the LVF deserves consideration as a major mechanical discontinuity instead of a simple rheological boundary, and second that taken alone within acceptable bounds the difference in rheology between the Peikang High and the deformed front belt zone cannot explain the total deviation observed in the velocity field of southern Taiwan. We infer that it is necessary to introduce some refinements in this model to account better for these velocity deviations.

3.4. Role of adjacent subduction

The counter-clockwise deviation of the velocity field in southern Taiwan may be due to the propagating tip of the collision zone, including the transition zone to the accretionary wedge between the Manila Trench to the west and the north Luzon Trough and Luzon volcanic arc to the east (see Fig. 1). We first tried to evaluate this effect in the finite-element modelling by adding a weak domain representing

Fig. 5. Symmetric preliminary 2-D finite-element model. (a) Rheology and boundary conditions: Young's modulus of 60 GPa for rigid subdomain (in grey) and 5 GPa for weak zone (in white). Poisson's ratio of 0.25 for both subdomains. Triangles represent fixed boundary; solid arrows, advancing boundary. (b) Computed velocity field. (c) Computed stress field, with principal stresses in the horizontal plane, shown as small couples of arrows (convergent arrows for maximum compressive stress).

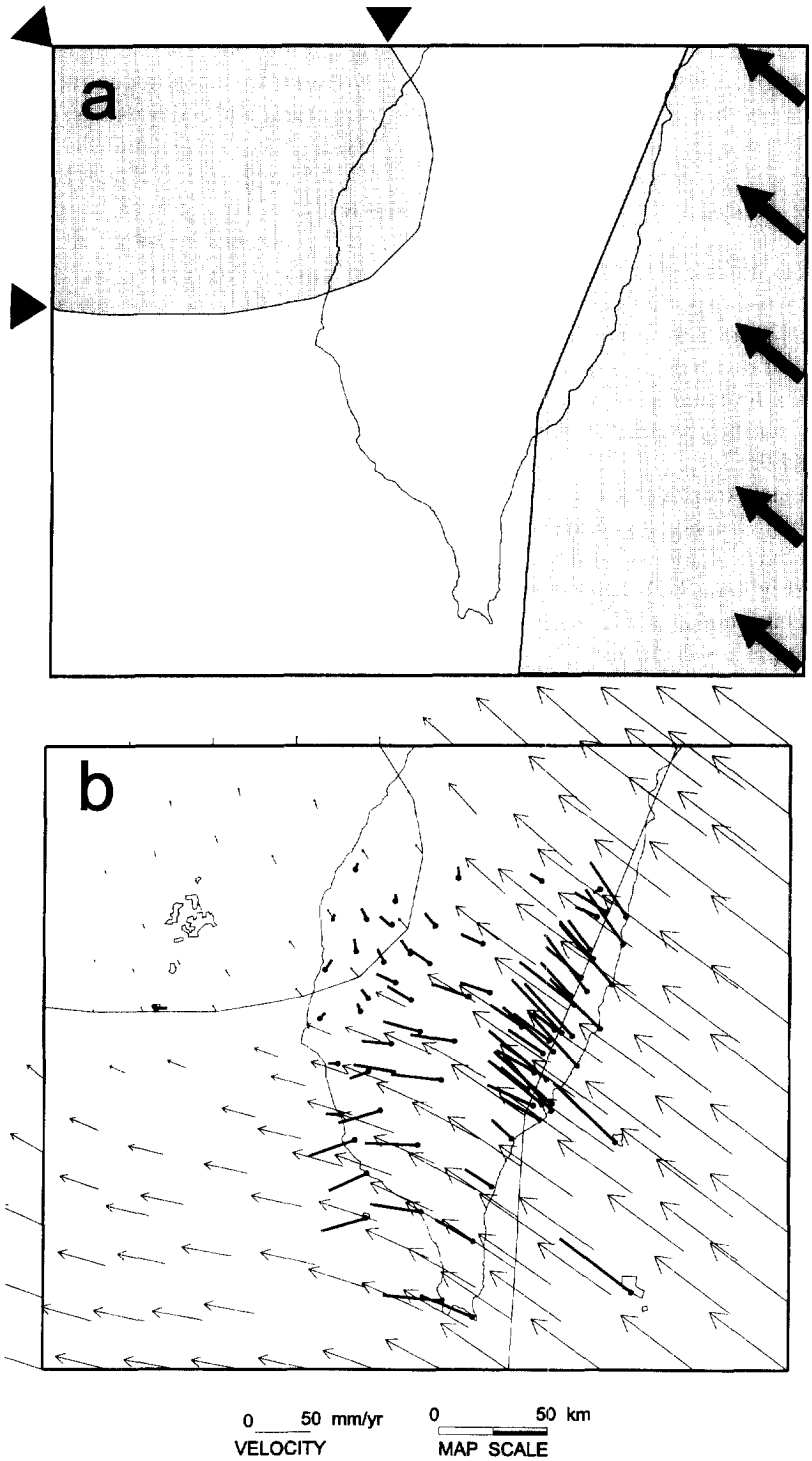

Fig. 6. Simple finite-element model of southwestern Taiwan. (a) Geometry and boundary conditions. Same rheologies and symbols as for Fig. 5. (b) Results of modelling and comparison with GPS data. Computed velocity vectors as thin arrows. Observed velocity vectors as thicker bars with dots indicating stations.

Table 1
Numerical values of mechanical and rheological parameters adopted in the models

	Block material properties	Joint material properties, no sliding	Joint material properties, sliding
Density	2700 kg m^{-3}	–	–
Young's modulus, E	60 GPa, 5 GPa	–	–
Poisson ratio, υ	0.25	–	–
Normal stiffness (GPa/m)	220	220	200
Shear stiffness (GPa/m)	220	220	198
Friction coefficient, μ	–	100	0.1

Young's modulus value is high (60 GPa) in shaded domains (Figs. 6a, 7a and 9) and low (5 GPa) in domain left white.

the deformable accretionary wedge: the results (not illustrated in this paper) revealed increasing counter-clockwise deviation of the velocity field in this area, relative to the model of Fig. 6. However, despite adoption of very weak rheology in this domain, the deviation obtained was never large enough to reproduce the ENE–WSW trends of velocity vectors observed in southwestern Taiwan (Fig. 3b).

3.5. Role of major discontinuities

We finally incorporated mechanical discontinuities in the distinct-element modelling (Fig. 7), in order to better account for the general structure shown in Figs. 1 and 2. These discontinuities are shown in Fig. 7 (note that the limit of the Peikang High, 1, is a simple rheological boundary, not a mechanical discontinuity; note also that the LVF, 4, is both a rheological boundary and a mechanical discontinuity, whereas there is no change in rheology across the discontinuities of the western thrusts, 2 and 3). This addition of 'weak' shear zones, however, was made gradually in order to avoid excessive complexity which would have resulted in poorer control of the different mechanical influences on the model inhomogeneity.

First, a single major discontinuity (the LVF of eastern Taiwan, 4 in Fig. 7a) was added. The velocity field obtained in this model (with the same boundary conditions as before) better accounted for the reality, especially for the E–W trends of velocity vectors on and off southwestern Taiwan (Fig. 3b). However, this model still failed to produce the ENE–WSW velocity vectors observed near Kaohsiung (Fig. 7a).

Second, we incorporated two additional discontinuities, 2 and 3 in Fig. 7b, which respectively correspond to the major front thrusts of the Taiwan belt, onland and offshore, and to the front of the Central Range (Fig. 1). The resulting model successfully reproduced nearly E–W and ENE–WSW velocity trending vectors in southwestern Taiwan, in agreement with the GPS observations (Fig. 7b).

Based on these experiments, we conclude that the presence of major front thrusts as well as that of the submarine accretionary wedge (Fig. 1) strongly influences the deviation of the velocity field in this region. Further sources of complexity do not deserve consideration, because their addition would not result in significant improvement of the fit, considering the level of detail and accuracy presently available in the geodetic network (Fig. 3).

3.6. The final distinct-element model

Taking into account both the simplifying assumptions of the numerical modelling and the various sources of uncertainties, the azimuthal fit between the GPS results and the final modelling (Fig. 7b) is rather good in the eastern and southwestern regions of Taiwan. In terms of azimuthal distribution, some local misfits are still observable, especially around the Peikang High area. The vectors obtained from GPS analyses show stronger deviations than those of our final model, which may be explained by both the role of local faults and the presence of lateral extrusion processes near the Peikang High due to indentation.

To constrain our model, we principally used the velocity field reconstructed by geodetic means. The fit, therefore, must be considered in terms of velocity magnitudes as well as velocity trends. In the previous subsections, trends have been examined, not magnitudes. Considering magnitudes, there is a general agreement between the regional distributions of

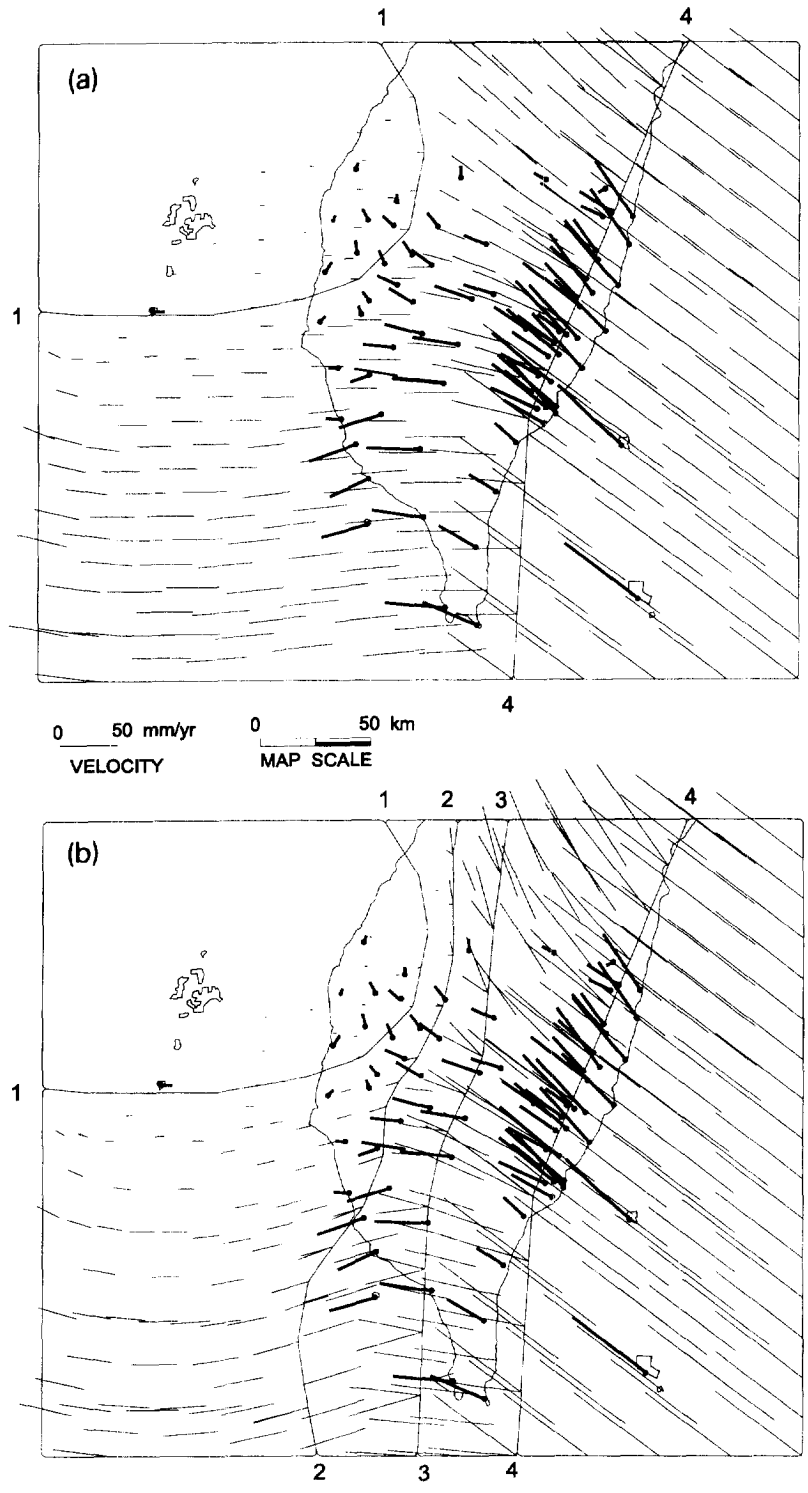
(a)
1
4
1
4
0 50 mm/yr
VELOCITY
0 50 km
MAP SCALE
(b)
1 2 3 4
1
2 3 4

computed and observed velocities (compare vector lengths in Fig. 7b). We thus observe that the largest azimuthal misfits (at the eastern tip of the Peikang High promontory) occur for the smallest observed and simulated velocities. Because these velocities were insignificant to marginally significant according to the GPS uncertainty estimates discussed in a previous section (Fig. 3), the azimuthal misfits cannot be considered significant either. Minor perturbations dependent on local structure are likely to occur near the Peikang High, but they cannot be considered at the scale of our model (Fig. 7b).

3.7. Influence of oblique discontinuities: 2-D vs. 3-D

Is the 2-D approximation reasonable for solving 3-D geodynamic problems? It implies drastic simplification (such as neglecting the vertical change of the rheological properties and the dips of major structures). Concerning the convergent boundary in Taiwan, however, the situation is essentially 3-D because major discontinuities are not vertical.

The major boundary, the active LVF, is a thrust with a left-lateral component (Hsu, 1976; Barrier and Angelier, 1986); its dip angle is about 55° (Tsai et al., 1977). In the 2-D modelling described above, this weakness zone is implicitly considered vertical. To elucidate the role of this dipping surface, a 3-D approach is compulsory while modelling the plate convergence in Taiwan. Such a 3-D modelling not only reveals new insights in terms of stress–strain relationships but also aims at clarifying the significance and limitations of previous 2-D modelling. In order to evaluate the effects of the obliquity of this discontinuity, we carried out comparisons between 3-D distinct-element modelling experiments (Fig. 8 and Fig. 9a, b) and 2-D ones (Fig. 9c, d), in conditions kept similar otherwise.

The new model used in this comparison (Fig. 9) is a 3-D distinct-element model which includes two subdomains with different material properties, in order to represent the mechanical behaviour of different regions (Fig. 8). This configuration was chosen according to the regional structural framework of the area under investigation (Fig. 8a). In order to maintain a good control of different mechanical influences, the 3-D models used for the first-order approximation are simplified in comparison with not only the actual patterns but also the 2-D models previously discussed.

Fig. 9 shows the stress and displacement fields of the simplified 2-D model (Fig. 9a, b) and the corresponding 3-D model (Fig. 9c, d). Despite the 50° dip attributed to the LVF in the 3-D model (Fig. 8) in contrast with its implicit vertical attitude in the 2-D model, the results are nearly equivalent. We effectively obtained similar stress fields (Fig. 9a, c) and similar deformation fields (Fig. 9b, d). We conclude that the 2-D approximation is a reasonable simplification in this case. This conclusion is important in practice, because the 2-D numerical modelling is much easier to handle and enables one to use more sophisticated representation of regional patterns than the 3-D modelling for a similar memory size and run time.

4. Discussion and conclusion

The new distinct-element modelling presented in this paper (Figs. 7 and 9) principally aimed at understanding the relationships between the regional sources of inhomogeneity (promontory, obliquity of motion and sinuous shape of boundary, presence of large and narrow weakness zones) and the displacement field, within the frame of the active Taiwan collision. Our modelling took advantage of the recent GPS analyses in Taiwan (Yu and Chen, 1994; Yu et al., 1997). Had this reconstruction of the present-day displacement field not been done, our modelling would never have reached this level of detail in the absence of accurate constraints. It is also important to note that contrary to the azimuthal adjustments

Fig. 7. Distinct-element model of southwestern Taiwan. Geometry and boundary conditions not shown, for clarity: same as for Fig. 6. Rheological boundaries: *1* for Peikang High, *4* for Longitudinal Valley. (a) Model with a single discontinuity at Longitudinal Valley Fault (numbered *4*). Computed velocity vectors as thin lines. Observed velocity vectors as thicker bars with dots indicating stations. Mechanical properties (including mechanical discontinuities) listed in Table 1. (b) Model with three discontinuities: front thrust of the western Taiwan belt (*2*) with southward transition to the frontal portion of submarine accretionary wedge off Taiwan; *3* = thrust between Central Range and Western Foothills; *4* = Longitudinal Valley Fault. Other explanations as for (a).

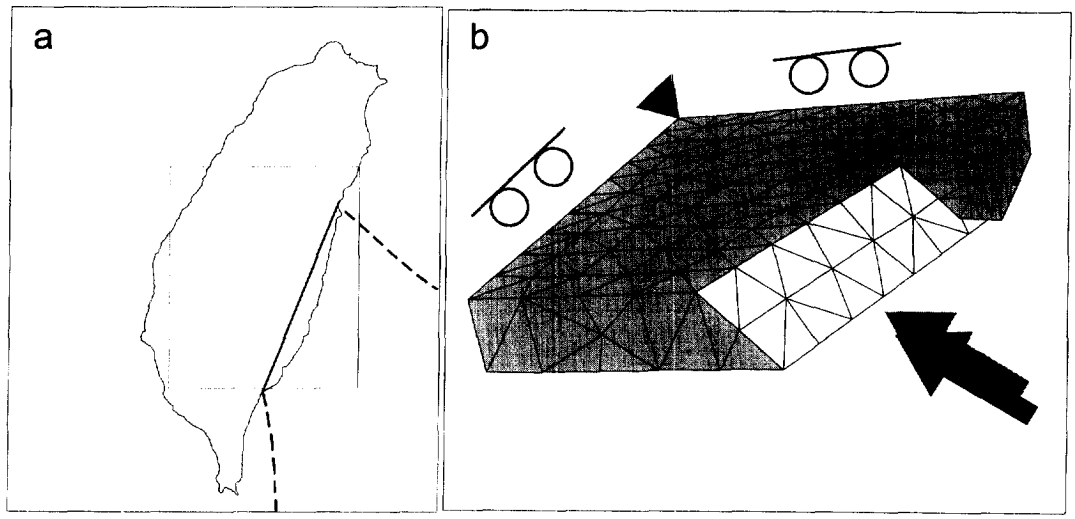

Fig. 8. The preliminary 3-D distinct-element model of Taiwan collision. (a) Location of the model in the map, with the main discontinuity as thick line. (b) Geometry and boundary conditions of the distinct-element model of eastern Taiwan, with eastern block (Philippine Sea plate) removed to show the dips of mechanical discontinuity. Boundary conditions: solid triangles, fixed corner; open circles with bar, roller in one direction; no symbol, free segments. Large arrow: direction of displacement (based on plate kinematics). Numerical values of mechanical and rheological parameters adopted in models: Young's modulus value is high (60 GPa) in removed domains and low (5 GPa) in the western domain. The Poisson ratio is 0.25. For joint material properties, see Table 1.

done in the past, our fits were considered in terms of velocity amplitudes as well as trends.

The 2-D finite-element elasto–plastic model previously presented by Hu et al. (1996) covered a much wider area, including not only the whole Taiwan orogen but also the neighbouring arc-and-trench systems (Fig. 10a). The main constraints used to adjust this general finite-element model came from the geological and geophysical reconstructions of stress fields in Taiwan (Angelier et al., 1986, 1990; Barrier and Angelier, 1986; Lee, 1986; Chu, 1990). The comparison between the observed and reconstructed stress fields is summarized in Fig. 10 (b and a, respectively). In Fig. 10b, an interpolation procedure proposed by Lee and Angelier (1994) was adopted to construct smoothed trajectories with large numbers of local palaeostress results. Several major geodynamic problems were addressed in this earlier modelling, including that of the relationships between the Taiwan collision, the Okinawa back-arc opening and the Ryukyu trench retreat, which strongly influence the distribution of strain–stress fields in northern Taiwan.

In counterpart, this finite-element modelling at the scale of several hundred kilometres (Fig. 10a) was unable to account for the deviations analysed herein at the scale of several tens of kilometres. The effects of mechanical decoupling across discontinuities were ignored, although they result in significant deviation of principal stress. These effects were taken into account in the new distinct-element modelling (Figs. 7b, 9 and 10c).

Considering the main shear zone of eastern Taiwan, the N50°W present-day plate motion vectors of the Philippine Sea plate make an angle of about 70° with the N20°E trend of the LVF. The ratio between the strike-slip (sinistral) and transverse (thrust) components of active motion of the LVF is 1 : 3, as revealed by local studies (Yu and Liu, 1989; Lee and Angelier, 1993). Mount and Suppe (1992) showed that the maximum horizontal stress trends also make high angles (70°–90°) with the trends of the active San Andreas Fault in California and the Great Sumatran Fault in Indonesia, because such large crustal-scale strike-slip faults may be inherently weak surfaces. Faulting and crustal deformation along such weak tectonic boundaries may be controlled by 'strong crust and weak transformation'. The shear stress in the crust appears to be generally high (i.e., consistent with Byerlee's law), whereas the shear stresses resolved on these bound-

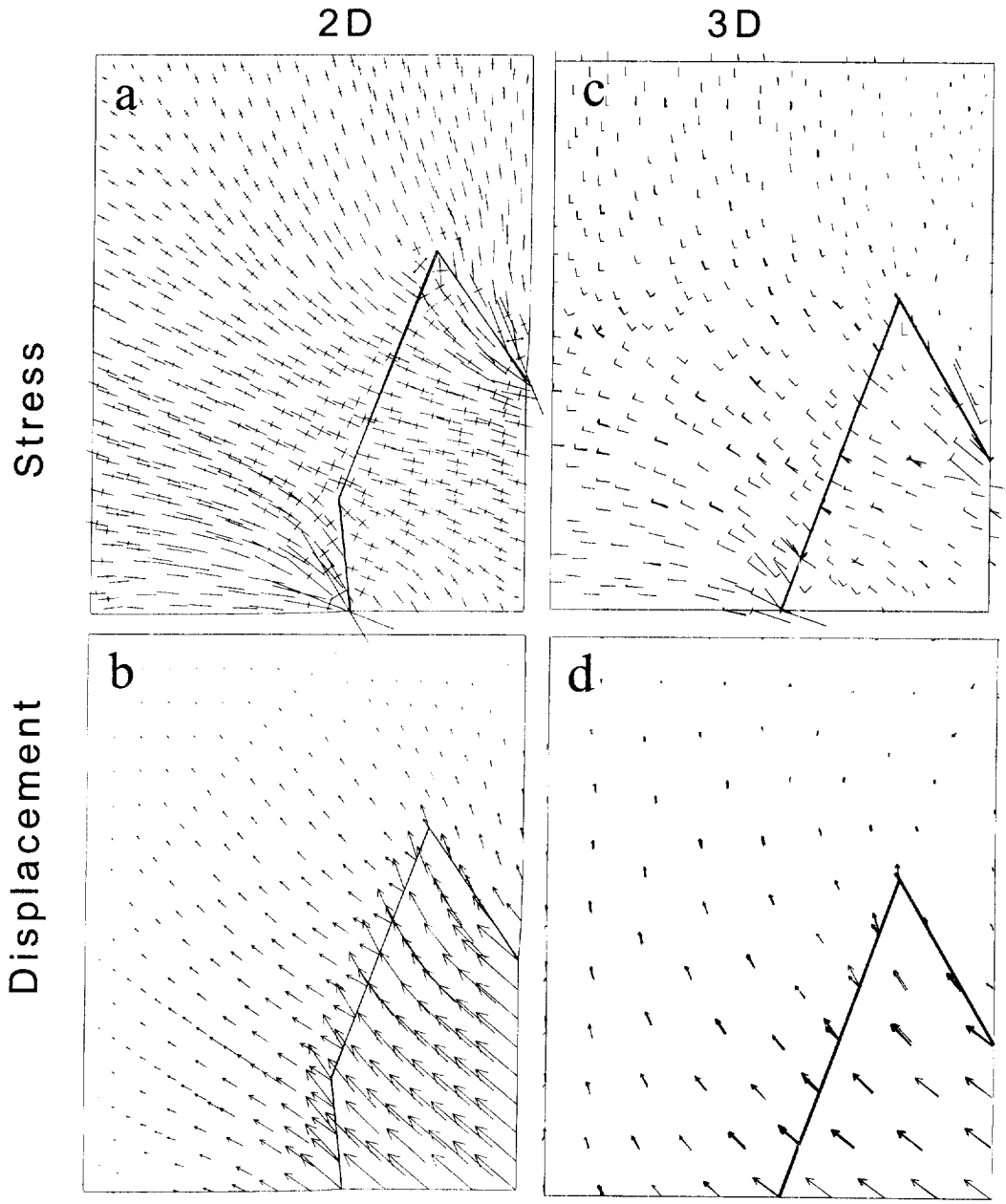

Fig. 9. 3-D and 2-D distinct-element models of eastern Taiwan. Location in Fig. 8a. (a) Computed stress distribution in 2-D model. (b) Trends of deformation fields in 2-D model. (c) Computed stress distribution in 3-D model. (d) Trends of deformation fields in 3-D model. The 3-D model is described in Fig. 8b.

ary strike-slip faults are low. The case discussed here is different, because the major active boundary, the LVF, is not a pure strike-slip fault but a thrust with a minor left-lateral component (Hsu, 1976; Barrier and Angelier, 1986). As a result, the mechanical coupling is probably higher than in the cases mentioned above. Significant mechanical decoupling may however occur along the LVF, explaining the systematic

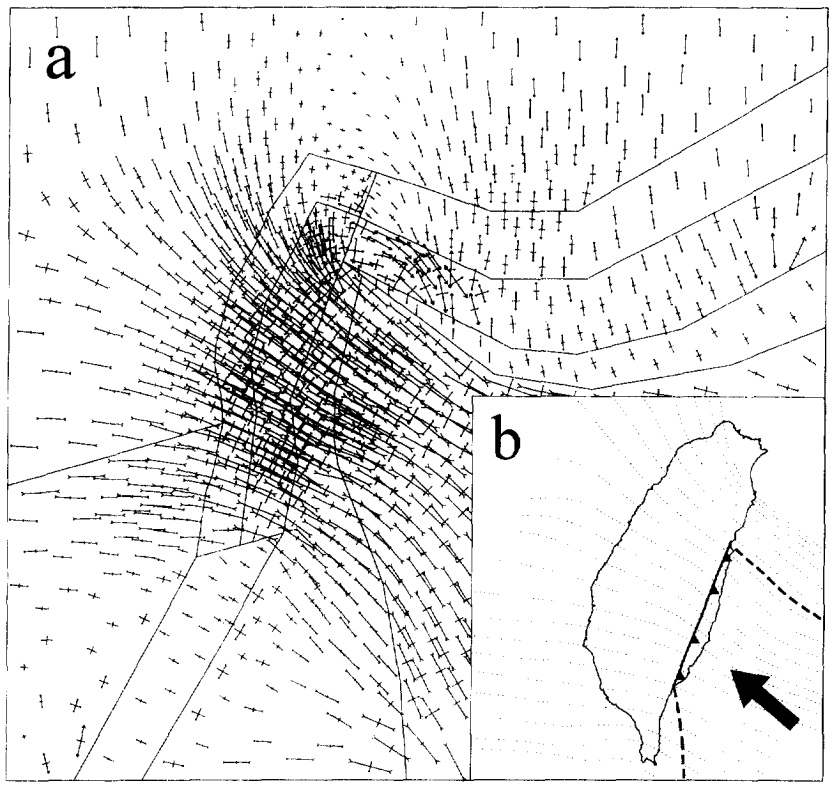
a
b

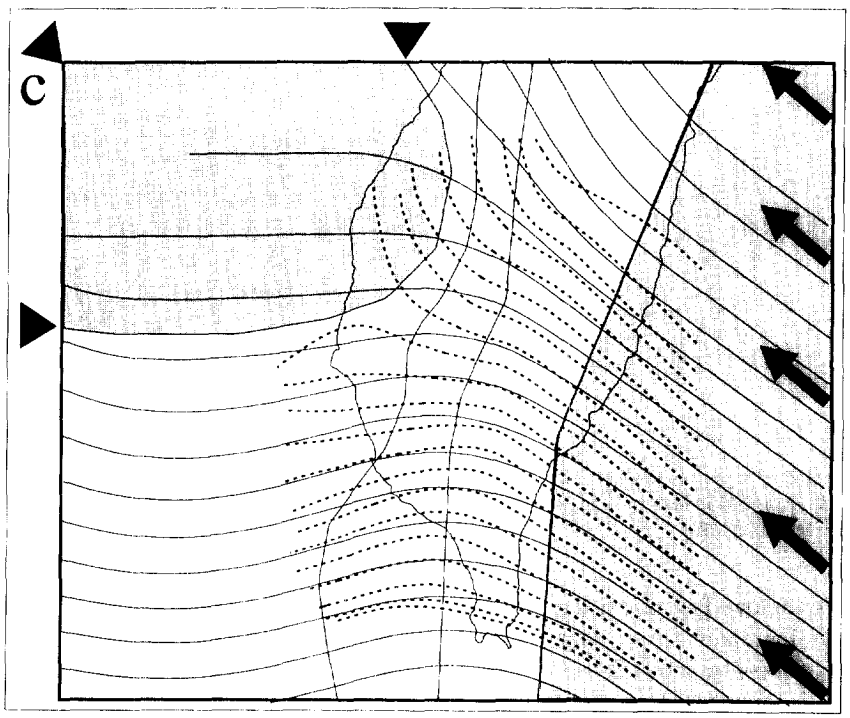
c

regional counter-clockwise deviation of compressional stress trajectories west of the LVF. This effect was partly reproduced in the distinct-element modelling (Fig. 9).

The results of our final distinct-element model of the deformation of southern Taiwan are summarized in Fig. 10c, which shows in terms of orientations how the computed velocity field (trajectories as solid lines) fits the observed one (trajectories as dashed lines). For the sake of simplicity, the velocity trajectories were drawn in the map of Fig. 10c based on the local determinations of Fig. 3b (observed) and Fig. 7b (simulated), using the interpolation smoothing procedure proposed by Lee and Angelier (1994). Not surprisingly, the fit is satisfactory in terms of trends, because of the successive improvements presented in the preceding section of this paper. Considering the magnitude (Fig. 7b), the general fit appears still better. Not only the distributions of amplitudes are similar, as shown by the comparison between lengths of bars (observed vectors) and arrows (computed vectors) in Fig. 7b, but also the examination of the smallest velocities (at the southeastern tip of the Peikang High) reveals that the azimuthal misfits highlighted in the trajectories of Fig. 10c are in fact not significant (see confidence ellipses in Fig. 3 and previous discussion).

Across the western thrust faults, however, the distribution of displacement vectors in the model does not depict satisfactorily the drop in magnitude observed with the GPS data. Some local velocity misfits are as large as 10–20 mm/yr (Fig. 7). A problem with the 2-D approach is the choice of the structural pattern which best accounts for the real deformation occurring in an fold-and-thrust belt. The overthrusting in south Taiwan is 3-D problem. The vertical components of the thrust displacements are significant compared to the horizontal components (Fig. 1a). Therefore, the modelling of this situation with a 2-D code is not quite appropriate, even when the thin-plate approximation is used. Especially, the implicit use of vertical discontinuities is of course not appropriate for modelling the behaviour of inclined thrusts. This problem was addressed before using 3-D distinct-element modelling (Figs. 8 and 9) applied to the LVF, a fault oblique to the Earth's surface with a slip vector oblique to fault strike. For most thrust faults of western Taiwan, the strike-slip component of motion is minor. This aspect is highlighted by the GPS analysis for the Foothills thrust zones (compare Fig. 3b with Figs. 1 and 2). The discontinuities used in the 2-D modelling accommodate lateral motion, not perpendicular motion, relative to fault trends. This is not the case for the 3-D distinct modelling (Figs. 8 and 9c, d), which allows consideration of oblique movements and is thus indispensable.

The counter-clockwise deviation of displacement vectors and directions of compression observed in southwestern Taiwan are the most prominent regional feature observed from both the GPS velocity field reconstruction and the stress determinations (Figs. 3 and 4). From the structural point of view, it is accounted for by a significant component of left-lateral slip of the main thrusts, relative to the usual NNE–SSW trend of the fold-and-thrust belt. Our experiments indicated that several tectonic factors (the Peikang High, active regional discontinuities) concur to provide a mechanical explanation for this regional deviation (Figs. 6 and 7). These fac-

Fig. 10. (a) Stress distribution in and around Taiwan calculated with the 2-D convergence-trench retreat elasto–plastic model of Hu et al. (1996). Principal stresses in the horizontal plane shown as small couples of arrows. Pairs of convergent arrows represent maximum compressive stress. Pairs of divergent arrows represent minimum extensional stress (especially northeast of Taiwan, in the Okinawa Trough area). Thin lines indicate rheological boundaries; for structure, rheology and boundary conditions, see Hu et al. (1996). Note stress concentration in the Taiwan collision zone, fan-shaped distribution of compression throughout the island and pronounced stress trajectory deviation at the northwestern corner of the Philippine Sea plate. (b) Actual stress distribution reconstructed from Quaternary palaeostress and present-day stress analyses: main compressional stress field associated with the Quaternary collision from various sources (focal mechanisms, borehole breakouts and Quaternary fault slip data). Trajectories of compression as dotted lines, obtained with the interpolation method of Lee and Angelier (1994). Plate boundary added as thick line with triangles on the upthrust side. Vector of relative plate motion as large black arrow. For more details, see Hu et al. (1996). (c) Trends of velocity fields in the final distinct-element model (same model as for Fig. 7b). Trajectories shown for GPS velocity data (dashed lines, from Fig. 3) and computed velocities (thin continuous lines, from Fig. 7b). Trajectories obtained with the interpolation method of Lee and Angelier (1994). Boundary conditions and rheological properties also illustrated (as for Fig. 6, see also Table 1). Mechanical discontinuities: see lines 2, 3, and 4 in Fig. 7b.

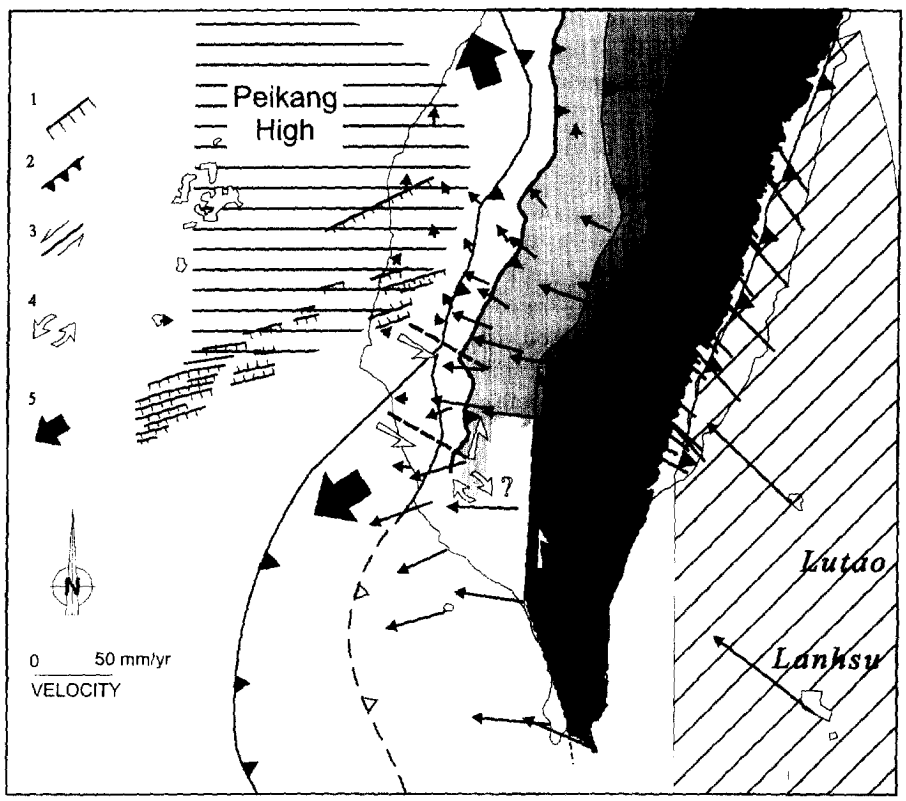

Fig. 11. Proposed geodynamic model of the active deformation of southern Taiwan. Numbers: *1* = normal fault; *2* = thrust fault; *3* = strike-slip fault; *4* = block rotation; *5* = tectonic escape. Main structural units, see Fig. 1a. GPS velocity vectors as thin arrows.

tors were separately studied in previous geological studies which highlighted the geological reality of several aspects. The role of the tectonic extrusion affecting the front zone of the fold-and-thrust belt around the Peikang High was studied by Lu (1994) following analogic modelling experiments made by Lu and Malavieille (1994). Some palaeomagnetic studies in the Foothills also supported the interpretation in terms of southward propagating clockwise rotation of thrust units, although this conclusion is still uncertain because magnetic minerals in mudstone series poorly recorded rotation (Horng, 1991). Note, in contrast, that AMS studies clearly confirm the N100–110° trend of recent compression in southwestern Taiwan. The tectonic analysis of southward propagating folds and thrusts, as well as the identification of a major NW–SE-trending transfer fault zone near the front of the belt (Deffontaines et al., 1997), also confirm this interpretation in terms of regional counter-clockwise deviation of compression related to the behavior of structural discontinuities, reverse and strike-slip in type. This general interpretation is summarized in Fig. 11. We conclude that the clockwise rotation of the displacements in southwestern Taiwan, which is explained by the general mechanical behaviour of the collision zone, is also mechanically consistent with the tectonic behaviour of individual geological units.

We conclude that under certain limitations the presence of 'weak' mechanical discontinuities is well accounted for by distinct-element modelling, and that this new modelling is particularly suitable in the case of southern Taiwan, where several sources of inhomogeneity concur to produce complex deformation. These sources are related not only to the presence of a relatively rigid promontory at the front of the active belt (the Peikang High), but also to the existence of a weak domain to the south (the accretionary prism at the northern tip of the Manila subduction zone) and of several major 'weak' shear

zones (the front thrusts of the Taiwan belt to the west and the LVF to the east).

In this new modelling, the level of detail increased because of the tighter constraints brought by recent GPS analyses of active deformation; however, numerous local deviations of the velocity and stress fields are still out of reach in modelling because their analysis would require a smaller spacing of geodetic control points. It should be noticed, however, that the higher precision also results from the use of the distinct-element method, because perturbations induced by narrow shear zones are now considered.

Finally, our modelling indicates that the present-day velocity field in southwestern Taiwan strongly depends not only on the geometry of the plate boundary, the direction of plate convergence and the presence of basement highs within the Chinese margin (also consistent with the crescent shape of the thrust wedge and the presence of transpression or transtension structures), but also on the presence of major zones of relative weakness and mechanical decoupling. The influence of slip along large 'weak' shear zones on the regional tectonic patterns of strain and stress is thus highlighted in the case of the Longitudinal Valley Fault zone and the western thrusts of the belt. Likewise, the strong deviation illustrated by E–W and ENE–WSW trends of velocity vectors in southwestern Taiwan (Fig. 3) probably results from the presence of the wide submarine fold-and-thrust zone and accretionary wedge, as a domain of mechanical weakness at the southern extremity of the Taiwan collision zone.

Acknowledgements

We are grateful to A. Poliakov and two anonymous reviewers for their constructive and helpful comments. Special thanks are due to Dr. C.J. Lee and H.T. Chu for stimulating discussion. The support from the I.F.T.–N.S.C. cooperation framework (Institut Français à Taipei and National Science Council of Taiwan) for field work, and from the French I.F.P. (Institut Français du Pétrole) for modelling expenses are gratefully acknowledged. The help of the C.R.O.U.S. in Paris and the Ministry of Education in Taipei was much appreciated. This is a contribution of the Institute of Earth Sciences, Academia Sinica, IESEP97-002.

References

Angelier, J., 1979. Determination of the mean principal direction of stress for a given fault population. Tectonophysics, 56: T17–T26.

Angelier, J., 1984. Tectonic analysis of fault slip data sets. J. Geophys. Res., 89: 5835–5848.

Angelier, J., 1986. Preface. Geodynamics of the Eurasia–Philippine Sea plate boundary. Tectonophysics, 125: IX–X.

Angelier, J., Bergerat, F. and Chu, H.T., 1986. Plate collision and paleostress trajectories in a fold-and thrust belt: the Foothills of Taiwan. Tectonophysics, 125: 161–178.

Angelier, J., Bergerat, F., Chu, H.T. and Lee, T.Q., 1990. Tectonic analysis and the evolution of a curved collision belt: the Hsüehshan Range, northern Taiwan. Tectonophysics, 183: 77–96.

Barrier, E., 1985. Tectonique d'une chaîne de collision active: Taiwan. Mém. Sci. Terre, Univ. P. et M. Curie, Paris, 85-29, 492 pp.

Barrier, E., 1986. The double collision of Taiwan: an active orogen. Tectonophysics, 125: 39–72.

Barrier, E. and Angelier, J., 1986. Active collision in eastern Taiwan: the Coastal Range. Tectonophysics, 125: 39–72.

Chiu, H.T., 1973. Basements rocks under the Neogene formation of west-central Taiwan. Proc. Geol. Soc. China, 16: 51–58. Miocene stratigraphy and its relation to the Paleogene rocks in west-central Taiwan. Pet. Geol. Taiwan, 12: 51–80.

Chou, J.T., 1969. A petrographic study of the Mesozoic and Cenozoic rock formations in the Tungliang well TL-1 of the Penghu Islands, Taiwan, China: U.N. ECAFE Comm. for Coordination of Joint Prospecting for Mineral Resources in Asia Offshore Areas (CCOP), Tech. Bull., 2: 97–115.

Chu, H.T., 1990. Néotectonique cassante et collision plio–quaternaire à Taiwan. Mém. Sci. Terre, Univ. P. et M. Curie, Paris, 292 pp.

Cundall, P.A., 1971. A computer model for simulating progressive large scale movement in blocky rock systems. Symp. Soc. Int. Mec. Roches, Nancy, 1: 11–18.

Cundall, P.A., 1988. Formulation of a three dimensional distinct element model, Part I. A scheme to detect and represent contacts in a system composed of many polyhedral blocks. Int. J. Rock Mech. Min. Sci. Geomech. Abs., 25: 107–116.

Davis, J.L., Prescott, W.H., Svarc, J.L. and Wendt, K., 1989. Assessment of Global Positioning System measurements for studies of crustal deformation. J. Geophys. Res., 94: 13,635–13,650.

Deffontaines, B., Lacombe, O., Angelier, J., Chu, H.T., Mouthereau, F., Lee, C.T., Deramond, J., Lee, J.F., Yu, M.S. and Liew, P.M., 1997. Quaternary transfer faulting in Taiwan foothills: evidence from a multisource approach. In: S.E. Lallemand and H.-H. Tsien (Editors), Active Collision in Taiwan. Tectonophysics, 274: (this issue).

DeMets, C.R., Gordon, R.G., Argus, D. and Stein, S., 1990. Current plate motions. Geophys. J. Int., 101: 425–478.

Elishewitz, B., 1963. A new interpretation of the structure of the Miaoli area in the light of the décollement tectonics of northwestern Taiwan. Pet. Geol. Taiwan, 2: 2145.

George, P.L., Laug, P., Muller, B. and Vidrascu, M., 1986. Guide d'utilisation et normes de programmation, 1. Inst. National Recherche Informatique Automatique, Le Chesnay, 113 pp.

Hart, R., Cundall, P.A. and Lemos, J., 1988. Formulation of a three dimensional distinct element model, Part II. Mechanical calculations for motion and interaction of a system composed of many polyhedral blocks. Int. J. Rock Mech. Min. Sci. Geomech. Abs., 25: 117–125.

Ho, C.S., 1986. A synthesis of the geologic evolution of Taiwan. Tectonophysics, 125: 1–16.

Horng, C.S., 1991. Magnetic Mineralogy and Magnetostratigraphic Studies of the Tsengwenchi and Erhjenchi Sections, Southwestern Taiwan. Ph.D. dissertation, Inst. of Oceanography, National Taiwan Univ., 323 pp

Hsieh, S.H. and Hu, C.C., 1972. Gravimetric and magnetic studies of Taiwan. Pet. Geol. Taiwan, 10: 283–321.

Hsu, T.L., 1976. Neotectonics of the Longitudinal Valley, eastern Taiwan. Bull. Geol. Surv. Taiwan, 25: 53–62.

Hsu, S.K. and Sibuet, J.-C., 1995. Is Taiwan the result of arc–continent or arc–arc collision? Earth Planet. Sci. Lett., 136: 315–324.

Hu, J.C., 1995. Modélisation numérique et analyse tectonique régionale. Mém. Sci. Terre, Univ. P. et M. Curie, Paris, 268 pp.

Hu, J.C., Yu, S.B., Angelier, J. and Lu, C.Y., 1995. An interpretation of the GPS velocity field of southern Taiwan based on numerical modelling. ACT Int. Conf., Ext. Abstr. Geol. Soc. China Spec. Publ., Taipei, pp. 141–149.

Hu, J.C., Angelier, J., Lee, J.C., Chu, H.T. and Byrne, D., 1996. Kinematics of convergence, deformation and stress distribution in the Taiwan collision area: 2-D finite-element numerical modelling. Tectonophysics, 255, 243–268.

Huang, C.Y., Shyu, C.T., Lin, S.B., Lee, T.Q. and Sheu, D.D., 1992. Marine geology in the arc–continent collision zone off southern Taiwan: implication for late Neogene evolution of the Coastal Range. Mar. Geol., 107: 183–212.

Huang, C.Y., Yuan, P.B., Song, S.R., Lin, C.W., Wang, C., Chen, M.T., Shyu, C.T. and Karp, B., 1995. Tectonics of short-lived intra-arc basins in the arc–continent collision terrane of the Coastal Range, eastern Taiwan. Tectonics, 14: 19–38.

Huang, T.C., 1978. Calcareous nannofossils of the subsurface pre-Miocene rocks from the Peikang basement high and adjacent areas in western-central Taiwan (part I. Cretaceous). Pet. Geol. Taiwan, 15: 49–87,

Huchon, P., 1986. Comment on 'Kinematics of the Philippine Sea plate' by B. Ranken, R.K. Cardwell and D.E. Karig. Tectonics, 1: 165–168.

Huchon, P., Barrier, E., De Bremaecker, J.C. and Angelier, J., 1986. Collision and stress trajectories in Taiwan: a finite element model. Tectonophysics, 125: 179–191.

Lacombe, O., Angelier, J. and Laurent, P., 1993. Les macles de la calcite, marqueurs des compressions récentes dans un orogène actif: l'exemple des calcaires récifaux du Sud de Taiwan. C.R. Acad. Sci. Paris, 316, Sér. II : 1805–1813.

Lee, C.T., 1986. Methods of Stress Analysis and Paleostress Changes in Northern Taiwan Due to Arc–Continent Collision. Unpubl. Ph.D. thesis, National Taiwan University, Taipei, 370 pp. (in Chinese).

Lee, J.C. and Angelier, J., 1993. Localisation des déformations actives et traitements des données géodésiques: l'example de la faille de la Vallée Longitudinal, Taïwan. Bull. Soc. Géol. Fr., 164(4): 533–570.

Lee, J.C. and Angelier, J., 1994. Paleostress trajectories maps based on the results of local determinations: the 'lissage' program. Comput. Geosci., 20(2): 161–191.

Liu, C.S., Lundberg, N., Reed, D.L. and Huang, Y.L., 1993. Morphological and seismic characteristics of the Kaoping Submarine Canyon. Mar.Geol., 111: 93–108.

Lu, C.Y., 1994. Neotectonics in the foreland thrust belt of Taiwan. Pet. Geol. Taiwan, 29: 1–26.

Lu, C.Y. and Hsü, K.J., 1992. Tectonic evolution of the Taiwan Mountain Belt. Pet. Geol. Taiwan, 29: 15–35.

Lu, C.Y. and Malavieille, J., 1994. Oblique convergence, indentation and rotation tectonics in the Taiwan Mountain Belt: insights from experimental modelling. Earth Planet. Sci. Lett., 121: 477–494.

Lu, C.Y., Angelier, J., Chu, H.T. and Lee, J.C., 1995. Contractional, transcurrent, rotational and extensional tectonics: a case study in northern Taiwan. Tectonophysics, 246: 129–146.

Lundberg, N., Reed, D.L. and Liu, C.S., 1991. The submarine propagation tip of the Taiwan collision: shallow crustal structure and orogenic sedimentation. In: C.T. Shyn, Y. Huang and Y.T. Yeh (Convenors), Proc. TAICRUST workshop. Natl. Taiwan Univ., Taipei, pp. 93–102.

Matsumoto, R., 1965. Some molluscan fossils from the buried Cretaceous of western Taiwan. Pet. Geol. Taiwan, 4: 1–24.

Meng, C.Y., 1967. The structural development of the southern half of Taiwan. Proc. Geol. Soc. China, 10: 77–82.

Minster, J.B. and Jordan, T.H., 1979. Rotation vectors for the Philippine and Rivera plates. EOS, Trans. Am. Geophys. Union, 60: 958.

Mount, V.S. and Suppe, J., 1992. Present-day stress orientation adjacent to active strike-slip faults: California and Sumatar. J. Geophys. Res., 97: 11,955–12,013.

Ranken, B., Cardwell, R.K. and Karig, D.E., 1984. Kinematics of the Philippine Sea plate. Tectonics, 3: 555–575.

Rocher, M., Lacombe, O., Angelier, J. and Chen, H.-W., 1996. Mechanical twin sets in calcite as markers of recent collisional events in a fold-and-thrust belt: Evidence from the reefal limestones of southwestern Taiwan. Tectonics, 15: 984–996.

Rothacher, M., Beutler, G., Gurtner, W., Bockmann, E. and Mervart, L., 1993. Documentation for Bernese GPS software v.3.4. Astronomical Institute, Univ. of Berne, 247 pp.

Seno, T., 1977. The instantaneous rotation vector of the Philippine Sea plate relative to the Eurasian plate. Tectonophysics, 42: 209–226.

Seno, T., Stein, S. and Gripp, A.E., 1993. A model for the motion of the Philippine Sea plate consistent with NUVEL-1 and geological data. J. Geophys. Res., 98: 17,941–17,948.

Stach, L.W., 1957. Stratigraphic subdivision and correlation of the upper Cenozoic sequence in the Foothills region of Chiayi and Hsinying, Taiwan. Symp. Petroleum Geology of Taiwan. Chinese Petroleum Corporation, Taipei, pp. 179–230.

Sun, S.C., 1965. On the occurrence of an unconformity in the

upper Miocene Wushan Formation and Kaitzuliao Shale near Shengshui-Tsun, Kaohsiung, Taiwan. Proc. Geol. Soc. China, 8: 100–101.

Suppe, J., 1984. Kinematics of arc–continent collision, flipping of subduction, and back-arc spreading near Taiwan. Mem. Geol. Soc. China, 6: 21–33.

Suppe, J., Hu, C.T. and Chen, Y.J., 1985. Present-day stress direction in western Taiwan inferred from borehole elongation. Petrol. Geol. Taiwan, 21: 1–12.

Teng, L.S., 1990. Geotectonic evolution of late Cenozoic arc–continent collision in Taiwan. Tectonophysics, 183: 57–76.

Tsai, Y.B., 1986. Seismotectonics of Taiwan. Tectonophysics, 125: 17–37.

Tsai, Y.B., Teng, T.L., Chiu, J.M. and Liu, H.L., 1977. Tectonic implications of the seismicity in the Taiwan region. Mem. Geol. Soc. China, 2: 13–41.

Yang, K.M., Ting, H.H. and Yuan, J.W., 1991. Structural styles and tectonic modes of Neogene extensional tectonics in southwestern Taiwan: implications for hydrocarbon exploration. Pet. Geol. Taiwan, 26: 1–31.

Yeh, Y.H., Barrier, E., Lin, C.H. and Angelier, J., 1991. Stress tensor analysis in the Taiwan area from focal mechanisms of earthquakes. Tectonophysics, 200: 267–280.

Yu, S.B. and Chen, H.Y., 1994. Global Positioning System measurement of crustal deformation in the Taiwan arc–continent collision zone. Terrestrial, Atmospheric and Oceanic Sciences (TAO), 5: 477–498.

Yu, S.B. and Liu, C.C., 1989. Fault creep on the central segment of the Longitudinal Fault, eastern Taiwan. Proc. Geol. Soc. China, 32(3): 209–231.

Yu, S.-B., Chen, H.-Y. and Kuo, L.-C., 1997. Velocity field of GPS stations in the Taiwan area. In: S.E. Lallemand and H.-H. Tsien (Editors), Active Collision in Taiwan. Tectonophysics, 274: 41–59 (this issue).